Chemical expansion of La0.8Sr0.2Fe0.7Ga0.3O3-δ

Olivier Valentin, Francis Millot, Eric Blond, Nicolas Richet, Aurélie Julian, Emmanuel Véron, Sandra Ory

Chemical expansion of $La_{0.8}Sr_{0.2}Fe_{0.7}Ga_{0.3}O_{3-\delta}$

Olivier Valentin[a], Francis Millot[b], Éric Blond[a], Nicolas Richet[c], Aurelie Julian[d], Emmanuel Véron[b], Sandra Ory[b]

Corresponding author: eric.blond@univ-orleans.fr, (+33) 02 38 49 43 58

[a] Institut PRISME EA 4229, University of Orléans, Polytech'Orléans, 8 rue L. de Vinci, 45072 Orléans, France

[b] CEMHTI - UPR3079 - CNRS, 1d Avenue de la Recherche Scientifique, 45071 Orléans Cedex 2, France

[c] Air Liquide CRCD, 1 chemin Porte des Loges BP126, 78354 Jouy en Josas, France

[d] SPCTS (UMR 6638 CNRS / University of Limoges); 47 av. A. Thomas, 87065 Limoges, France

Abstract: This paper deals with the chemical expansion measurements and modelling of $La_{0.8}Sr_{0.2}Fe_{0.7}Ga_{0.3}O_{3-\delta}$. The expansion behaviour has been evaluated using a dilatometer and X-ray diffraction over a wide range of temperatures (RT to 1373 K) and oxygen partial pressures (10^{-21} to 1 atm). The material stoichiometry evolution with temperature and oxygen partial pressure has been measured using thermogravimetry analysis at different oxygen partial pressure, from 10^{-21} to 0.5 atm and from RT to 1473 K. Considering a typical defect model for lanthanum ferrite oxides, chemical expansion depends linearly on the Fe^{4+} concentration rather than on the oxygen vacancy concentration. A model of chemical expansion as a function of pO_2 and temperature is then proposed. It helps to understand and anticipate the chemical expansion behaviour exhibited by this material when used as Ionic Transport Membrane (ITM).

Keywords: Chemical expansion, Ceramic Mixed Ionic and Electronic Conductors, Perovskite, Catalytic membrane reactor, Synthesis gas

1. Introduction

Mixed ionic and electronic conductors (MIECs) may be one solution to produce high purity hot oxygen. Such type of membranes could replace Air Separation Unit (ASU) for production of oxygen in the Partial Oxidation of Methane (POM) to syngas (H_2/CO) process. Energy-savings are expected compare to ASU based process [1, 2, 3]. The semi-permeability of oxygen through MIECs occurs at high temperature (873 - 1173 K) under a gradient of chemical potential between oxidizing and reducing side. Oxygen diffusion is possible due to the presence of oxygen vacancies (Schottky defects) and electron holes. Mixed conducting oxides having a ABO_3 perovskite structure have considerable interest for oxygen membrane separation. During the last two decades, numerous studies focused on materials development combining oxygen flux performance, mechanical stability, low chemical expansion coefficient and price. Here, the material of the membrane has a perovskite structure of chemical composition $La_{0.8}Sr_{0.2}Fe_{0.7}Ga_{0.3}O_{3-\delta}$, referred to as LSFG later in the text. This material presents a good compromise between oxygen permeation fluxes and mechanical stability [4, 5, 6].

During operation in a catalytic membrane reactor, the evolution of oxygen stoechiometry in the membrane induces a chemical expansion leading to chemo-mechanical stresses [7]. Chemical expansion from air to nitrogen atmosphere is of the same order as the thermal expansion for a temperature variation of 100 K, that is to say a strain around 10^{-4} [8]. In the POM process, the oxygen partial pressure is at on side air and at the other side methane. That means a gradient of 20 orders of magnitude resulting in stresses between both sides of the membrane. These chemo-mechanical stresses affect the mechanical reliability of the whole structure. They are identified as one of the main cause of failure [9] and an important problem for ITM reactor operation [10]. Considering material choice and mechanical stress predictions, the chemical expansion behaviour of the membrane must be understood and quantified as a function of operating parameters: oxygen partial pressure and temperature.

Many works have investigated the origin of the chemical expansion. It is related to cations size variations or/and to the modification of the Coulomb repulsion between the defects induced by oxidation and reduction of the material [7, 11, 12, 13]. Various approaches to describe chemical expansion exist in the literature. A classical models use a linear relation between oxygen vacancies concentration and chemical expansion ε_c [8, 13, 14, 15, 16, 17]:

$$\varepsilon_c = C \times (\delta - \delta_0) \quad (1)$$

Where C is the coefficient of chemical expansion (CCE), δ is the oxygen vacancies

concentration and δ_0 is the reference oxygen vacancies concentration. This model is widely used in the field of new material development, as it is convenient to give a ranking of the materials according to their chemical expansion [18]. However, the effects of temperature and oxygen partial pressure do not appear directly in this model. Another approach is given by Krishnamurthy *et al.* [19] assuming Vegard's law for the dependence of the oxide's crystal lattice parameter with elements concentrations. Similarly, using a thermodynamic formalism, without mechanical stress and for an isotropic solid, Adler [20] expresses the uniaxial strain ε, as:

$$d\varepsilon = \left(\frac{\partial ln(V)}{\partial T} \right)_{x_v,P} dT + \left(\frac{\partial ln(V)}{\partial x_v} \right)_{T,P} dx_v \quad (2)$$

Where V is the specific volume, T is the temperature, P the total pressure and x_v is the oxygen vacancies mole fraction. This definition has the advantage to distinguish the thermal and chemical strains.

This paper contributes to the chemical expansion characterisation and modelling of LSFG material [5]. The relation between chemical composition variation and chemical expansion is used to propose a chemical expansion model as a function of oxygen partial pressure and temperature. The ability to describe the chemical expansion behaviour at high temperature is discussed.

2. Experimental

LSFG is provided by "Pharmacie Centrale de France" and is synthesized by spray pyrolysis. Powder is attrition-milled using ZrO_2 media in ethanol until a mean grain size of 0.3 µm is obtained. The powder is directly used for thermogravimetry and X-ray diffraction (XRD). The samples for dilatometry are bars (8 mm x 5 mm x 5 mm) and cylinders (5 mm diameter and 9 mm length). They are elaborated by tape-casting and sintered at 1523 K for 2 hours in air [4].

XRD patterns have been collected using a conventional θ-θ Bragg–Brentano configuration (Ni-filtered CuK$\alpha_{1,2}$) on a Bruker AXS D8 Advance diffractometer (Karlsruhe, Germany) fitted with a linear Vantec-1 detector. The diffractometer is equipped with an Anton Paar (Graz, Austria) oven chamber (model HTK 1200 N) able to reach temperatures up to 1473 K. The temperature has been calibrated from ambient to 1473 K following the dilatation of reference alumina specimen. A gas panel with three mass flow controllers allows switching and mixing H_2, N_2 and O_2 gases. The total flow rate of gases is chosen constant at 5 L/min during all the measurements. Oxygen partial pressure is monitored at the outlet of the XRD chamber with an oxygen gauge (JC48V, Setnag). The sample holder is a 10 mm diameter alumina pellet monocrystalline known to not react with the LSFG powder. Two series of experiments have been performed. First, XRD patterns are recorded on

the sample held at 1173 K under various atmospheres (N_2/O_2, $N_2/H_2/O_2$), then XRD patterns are done at different temperatures (293-1273 K) under air. For lower oxygen partial pressure tests ($pO_2 < 10^{-4}$ atm), the device is previously flown during one night. For each measurement, two consecutive XRD patterns are recorded at 15 minutes intervals in order to check that the equilibrium state is reached. The lattice parameters were refined using Le Bail's method with the Topas Bruker AXS (Version 4) software [21].

Dilatometries have been conducted with a Setaram Setsoft 2400 dilatometer from 293 to 1373 K and in the range of oxygen partial pressure [10^{-5}; 0.21] atm with O_2/N_2 gas mixtures. In the first set of experiments, samples were heated up at 4 K/min to 1173 K under air (100 mL/min) and held for two hours. Then, the gas was shifted to lower oxygen partial pressure (N_2/O_2 or H_2/Ar) with a flow rate of 100 mL/min, held for 8 hours under isothermal condition and finally cooled down under the same atmosphere. For each atmosphere a blank test was performed to limit any shift due to the dwell time. In a second set of experiments (non-isothermal tests), the sample is previously stabilized under air. The test consists in a heating/cooling cycle at a rate of 4 K/min under a fixed atmosphere. In the first test, the sample was placed under N_2 atmosphere, heated from 293 to 1373 K and finally cooled to 293 K. In the second test, the atmosphere was switched to air and the same heating and cooling procedure was performed.

The apparatus for thermogravimetric measurement is a Setsys Evolution 24 (Setaram) coupled with a gas panel. Mixed gases (H_2, H_2O, N_2 and O_2) are combined and an oxygen gauge (JC48V, Setnag) is used to check the oxygen partial pressure at the outlet of the furnace. The sample was placed in an alumina crucible. The difference in buoyancy, which depends on the various gas compositions and temperatures, is taken into consideration. First part of experiments is conducted taking 125.7 mg of LSFG powder. Then in a second set of experiments, the mass of LSFG is 120.0 mg. The accuracy is in the range of ± 10 µg for a sample of 100 mg. To be independent of the initial mass, the results are expressed in terms of relative mass variation. The sample is first heated from ambient to 1173 K in flowing air (30 mL/min). In order to cover a wide range of pO_2 (0.5 to 10^{-21} O_2 atm), measurements are conducted under different gas flows (N_2/O_2 or $N_2/H_2/H_2O$) from 1073 to 1473 K.

3. Chemical expansion

3.1. X-Ray diffraction

At ambient temperature, the diffraction peaks of LSFG have been indexed by Julian *et al.* [22] in a

monoclinic P2/m structure. At high temperature (1173 K), depending on the x and y doping amount the crystal structure of $La_{1-x}Sr_xFe_{1-y}Ga_yO_{3-\delta}$ can be rhombohedric or cubic [5, 8, 12]. The cells parameters from XRD are refined using R-3c and Pm3m crystal structures according to literature for various $La_{1-x}Sr_xFe_{1-y}Ga_yO_{3-\delta}$ compositions at 1173 K and all oxygen partial pressure [8]. Furthermore, as seen in Fig. 1, no difference with temperature for XRD patterns is noticeable. Consequently the structure is closely cubic or rhombohedric even at low temperature. In the XRD patterns, peaks at 41.5° come from monocrystalline alumina support. Diffraction data could also be refined using the rhombohedral space group R-3c below 673 K. A new phase, which has not been identified, is formed at lower oxygen partial pressure ($pO_2 < 10^{-19}$ atm). This phase disappears with the increase of the oxygen partial pressure. The X-ray diffraction patterns obtained at 1173 K are shown in Fig. 2.

Fig. 1 about here

Fig. 2 about here

There is a minor difference in cell volume variation with atmosphere or temperature between the two reported space groups (pm3m and r-3c). Then, for chemical strain evaluation with isotropic assumption, the choice of the structure has no effect on the results as shown in Fig. 3. Finally, the pm3m space group is chosen and the relative volume variation is evaluated using:

$$\frac{\Delta V}{V_0} = \frac{V - V_0}{V_0} \tag{3}$$

Where V and V_0 are respectively the actual volume and the cell reference volume (1173 K, under air). Assuming an isotropic chemical expansion, the uniaxial strain is deduced from the volume change of the lattice cell:

$$\varepsilon = \frac{1}{3}\frac{\Delta V}{V_0} \tag{4}$$

The X-ray results of chemical strain with pO_2 at 1173 K are discussed in the next section.

Fig. 3 about here

3.2. Dilatometries

Isothermal dilatometries are presented in Fig. 4. In air, the expansion from ambient temperature to 1173 K is linear and is mainly composed of thermal expansion. Indeed, as LSFG material is sintered under air, the initial oxygen activity in the material is in equilibrium with a pO_2 equal to 0.21 atm.

After 2 hours at 1173K the gas is shifted. The curves show the chemical expansion of the material until it is in equilibrium with the new pO_2 at constant temperature. The lower the oxygen partial pressure is, the higher the chemically expansion will be. No mechanical damage, that could affect the measurement, is observed on the samples after the completion of the test.

Fig. 4 about here

The non-isothermal dilatometry test is shown in Fig. 5. Two atmospheres have been consecutively tested during this cyclic test: the first thermal cycle (i.e. heating and cooling) has been realized under air while the second has been done under Nitrogen. The atmosphere change takes place at the end of the first dilatometry at 398 K. The details of the temperature and atmosphere cycle are given in the experimental section. Below 700 K, both expansion curves exhibits a quasi-linear expansion that is solely causes by temperature variation. Above 700 K, under N_2 the curve presents a progressive expansion while in air a strong contraction is recorded. This difference corresponds to the chemical expansion. It also can be observed that the chemical strain is reversible from air to N_2. Since the diffusion of oxygen is thermally activated, its contribution to the chemical strain is thermally activated too. So, below the activation temperature, the thermal expansion is the only responsible of strain.

Without crystal phase modification, the thermal expansion of a material in equilibrium with its surrounding atmosphere does not present a hysteresis between heating and cooling. So, the shape of the curve for the first heating under nitrogen leads to the conclusion that the equilibrium is not reached before 1373 K. While under air, the equilibrium seems to be reached faster. Finally, the equilibrium is always attained before the cooling down starts. According to this observation, the residual chemical expansion between air and N_2, at a fixed temperature, is identified as the difference between each cooling. At 1373 K, the chemical expansion is 0.085 %; 0.151 % at 1173 K and 0.234 % at 293 K. Chemical expansion magnitude between air and N2 decreases with the increase of the temperature. This confirms that the chemical expansion depends significantly on the temperature.

Fig. 5 about here

From the results of dilatometries and XRD, the chemical expansion measurements in relation to oxygen partial pressure are plotted in Fig. 6. The chemical expansion varies with pO_2 in the high oxygen partial pressure region, contrary to the low-pressure region where the chemical expansion reaches a plateau below 3×10^{-5} atm. Hendriksen *et al.* [24] assumes a similar behaviour on $La_{0.6}Sr_{0.4}Co_{0.2}Fe_{0.8}O_{3-\delta}$ by extrapolation of a defect model [25].

Fig. 6 about here

4. Oxygen vacancies concentration variation

Mass variations of $La_{0.8}Sr_{0.2}Fe_{0.7}Ga_{0.3}O_{3-\delta}$ powder exposed to 1173 K and pO_2 variations are shown in Fig. 7. A blank correction has been realized for each operating conditions. The mass of the sample stabilizes after 5 hours exposure to the new gases. The reference conditions for the sample weight are 1173 K in 0.176 atm pO_2. When a more oxidative atmosphere is introduced the mass increases, while it decreases with a more reductive one. There is no mass variation for samples exposed up to 0.5 atm. This indicates that the sample is saturated with oxygen above 0.176 atm. A difference of 0.04 % of relative mass variation is recorded between the first measurements at 0.176 atm and the last one at the same oxygen partial pressure. This indicates a very good reversibility of the process.

Fig. 7 about here

Fig. 8 about here

Fig. 8. presents the weight variations versus temperature for three different pO_2. The behaviours under pO_2 of 0.176 and 2 x 10^{-2} atm are very close while under 3 x 10^{-3} the mass variation is more significant. Taking the assumption that oxygen incorporation and release is the only origin of the mass variation, oxygen-vacancy concentration $\Delta\delta$ is given by:

$$\Delta\delta = \frac{\Delta w}{w_{LSFG8273}} \frac{M_{LSFG}}{M_{Oxy}} \tag{5}$$

Where Δw is the weight change of the sample, $w_{LSFG8273}$ is the sample weight, M_{Oxy} is the oxygen atomic weight and M_{LSFG} is the molar weight of LSFG. These variations are connected with the oxygen composition of LSFG at 1173 K by assuming that the inflexion point of the S curve of Fig. 9 correspond to $\delta = \frac{x}{2} = 0.1$, that is to say $La_{0.8}Sr_{0.2}Fe_{0.7}Ga_{0.3}O_{2.9}$ composition [23, 26]. The results are related with this reference and are presented in Fig. 9. Gallium doping decreases the oxygen non-stoechiometry magnitude by comparison with $La_{0.6}Sr_{0.4}FeO_{3-\delta}$ studied by Sogaard *et al.* [23]. The substitution of iron by gallium, which is monovalent, could explain this difference.

Fig. 9 about here

The thermogravimetric analysis under 0.176, 2 x 10^{-2} and 3 x 10^{-3} atm are shown Fig. 10. The oxygen non-stoechiometry varies almost linearly with the temperature above 893 K. The curves are nearly parallel indicating a constant gap in oxygen stoichiometry from 893 to 1473 K. The oxygen vacancy concentration increases when increasing the temperature or lowering the oxygen partial pressure.

Fig. 10 about here

The relation between chemical strain and oxygen non-stoechiometry presented in Fig. 11 is obtained by combining results of Fig. 6 and Fig. 9. The data presented are interpolation of TGA and

XRD measurements under the same pO_2 at 1173 K. A non-linear behaviour of the chemical expansion ε_c with δ is found: above 0.1 oxygen vacancy concentration, the chemical expansion reaches a plateau.

Fig. 11 about here

5. Theory and modelling

5.1. Defect model

The oxygen non-stoechiometry δ in $La_{0.8}Sr_{0.2}Fe_{0.7}Ga_{0.3}O_{3-\delta}$ can be described with a point defect model [8, 27, 28]. As the oxide state of gallium is constant, the lanthanum ferrite is used as the reference composition. The majors defects in $La_{1-x}Sr_xFeO_{3-\delta}$ are $V_O^{\bullet\bullet}$, $Fe_{Fe}^{\bullet}$ and Fe'_{Fe} and Sr'_{La} with the Kröger-Vink notation. Mizusaki *et al.* have shown that the S shape of the $\mathrm{Log}\,\delta$ vs. $\mathrm{Log}\,pO_2$ curve at T can be divided into two distinct domains corresponding to the equilibrium between different defects [28]. These regions are plotted in Fig. 12. Region I corresponds to the equilibrium Fe^{4+}/Fe^{3+} and oxygen vacancies at high pO_2 while the region II corresponds to the equilibrium Fe^{3+}/Fe^{2+} and oxygen vacancies at low pO_2. In the transition region, the complex equilibrium between $Fe^{4+}/Fe^{3+}/Fe^{2+}$ must be considered. The corresponding defect equilibriums are established by means of the defect reactions (6) (regions I) and (7) (region II):

$$2Fe_{Fe}^{\bullet} + O_O^X \leftrightarrow \frac{1}{2}O_2 + V_O^{\bullet\bullet} + 2Fe_{Fe}^X \tag{6}$$

$$2Fe_{Fe}^X + O_O^X \leftrightarrow \frac{1}{2}O_2 + V_O^{\bullet\bullet} + 2Fe'_{Fe} \tag{7}$$

The oxygen vacancy concentration $\left[V_O^{\bullet\bullet}\right]$ is called δ. The concentrations of each species are determined through mass balance, site conservation and electro-neutrality conditions, which are for the defect reaction (6):

$$\left[O_O^X\right] = (3-\delta) \tag{8}$$

$$Fe_{Fe}^{\bullet} = Sr'_{La} - 2\left[V_O^{\bullet\bullet}\right] = 0.2 - 2\delta \tag{9}$$

$$Fe_{Fe}^{\times} = 1 - Fe_{Fe}^{\bullet} - Ga_{Ga} = 0.5 + 2\delta \tag{10}$$

And for the defect reaction (7):

$$Fe_{Fe}^{'} = 2\left[V_O^{\bullet\bullet}\right] - Sr'_{La} = 2\delta - 0.2 \tag{11}$$

$$Fe_{Fe}^{\times} = 1 - Ga_{Ga} - Fe_{Fe}^{'} = 0.9 - 2\delta \tag{12}$$

Considering $La_{0.8}Sr_{0.2}Fe_{0.7}Ga_{0.3}O_{2.9}$ as referenced composition, for ideally diluted defects the equilibrium constant of defect reactions (6) and (7) are:

$$K_{ox}(T) = \frac{\delta(0.5+2\delta)^2}{(3-\delta)(0.2-2\delta)^2}(pO_2)^{1/2} \quad (13)$$

$$K_{red}(T) = \frac{\delta(2\delta - 0.2)^2}{(0.9-2\delta)^2(3-\delta)}(pO_2)^{1/2} \quad (14)$$

Where K_{ox} is the equilibrium constant of the reaction (6) and K_{red} the equilibrium constant of the reaction (7).

Fig. 12 about here

After measurements of δ by thermogravimetry, the experimental data have been fitted with $K_{ox} = 0.15$ and $K_{red} = 1.44\times10^{-13}$ at 1173 K. As shown in Fig. 12, in the transition region, the defect structure consists mainly of 10 % oxygen vacancies. In order to extrapolate these measurements at 1173 K to other temperatures, the data collected under pO2 = 0.176, 2 x 10^{-2} and 3 x 10^{-3} atm between 293 and 1473 K have been used to calculate the standard enthalpy and entropy changes of the reactions. The evolution of the Gibbs free energy of a chemical reaction is given by:

$$-\Delta G_0 = RT\ln(K_{ox}) = -\Delta H_0 + T\Delta S_0 \quad (15)$$

where ΔH_0 is the evolution of standard enthalpy and ΔS_0 the evolution of standard entropy of the reaction (6) and T is the absolute temperature. The values of ΔH_0 and ΔS_0 have been determined by plotting the standard Gibbs free energy variation $RT\ln(K_{ox})$ versus T. The result is shown in Fig. 13. The corresponding enthalpy and entropy are reported in Tab. 1. The values are similar to values published by Sogaard *et al.* [23] and Mizusaki *et al.* [28] for LSF based perovskites. The linear dependence expected is observed for pO_2 0.176 and 2 x 10^{-2} in the range [900-1500] K. For 3 x 10^{-3} atm the linearity is only in the range 900 to 1300 K. Above 1300 K, as oxygen vacancies concentration reach a value between 0.8 and 0.9 while temperature increases, the material is in the transition region of the Fig. 9. Therefore, the chemical equilibrium is not governed any more solely by equation (6). This effect is also visible, for 2 x 10^{-2} atm at 1500 K: the corresponding data on Fig. 13 does not fit with the others. Indeed, the oxygen vacancies concentration at 1500 K for 2 x 10^{-2} atm corresponds to that for 3 x 10^{-3} atm at 1300 K (see Fig. 9).

Fig. 13 about here

Tab. 1 about here

5.2. Chemical expansion model

The origin of the chemical strain variation may be the change of oxygen vacancies concentration and the ionic radius differences among Fe^{2+}, Fe^{3+}, Fe^{4+} defect cations. The concentrations of defects are modified by the oxygen partial pressure of the surrounding atmosphere and by

temperature.

In the literature, the oxidation state of iron has been identified as the origin of chemical expansion [27]. From Fig. 11 and Fig. 12, since the chemical expansion varies only in the region I, the Fe^{4+}/Fe^{3+} equilibrium could yield the chemical expansion. The variation of chemical expansion as a function of $\left[Fe_{Fe}^{\bullet}\right]$ concentration is plotted in Fig. 14. It is obtained by combining the chemical expansion of Fig. 11 and $\left[Fe_{Fe}^{\bullet}\right]$ from equation (9).

Fig. 14 about here

The straight line matches the experimental points in the whole domain of compositions (from $pO_2=10^{-19}$ atm to $pO_2=1$ atm). It may be concluded that the chemical expansion varies linearly with the $\left[Fe_{Fe}^{\bullet}\right]$ concentration. The variation is much more important in the high-pressure region and very limited in the low-pressure region (region II), then it is possible to write:

$$\varepsilon_c = C \times \left(\left[Fe_{Fe}^{\bullet} \right] - f_0 \right) \tag{16}$$

Where C is the chemical expansion coefficient and $f_0 = \left[Fe_0^{4+}\right]$ is the concentration for a chemical expansion is null. It is found that $C = -0.014$ and the reference chemical expansion is chosen null for $pO_2=0.176$ at T=1173 K that corresponds to $f_0 = 0.117$. Armstrong *and al.* report a similar observation for doped lanthanum chromites where lattice expansion is related to the reduction of Cr^{4+} to Cr^{3+} to maintain electroneutrality under reducing environments [7]. This proportionality is also present in the work of Zuev *and al.* [29].

The objective of this work is to propose a model for chemical expansion as a function of the oxygen partial pressure and the temperature. A first remark is the direct relation between $\left[Fe_{Fe}^{\bullet}\right]$ and oxygen partial pressure and equilibrium constant $\left(pO_2, K_{ox}\right)$. Considering equation (9), equation (6) can be expressed according to $\left[Fe_{Fe}^{\bullet}\right]$:

$$K_{ox} = \frac{\left(0.1 - 0.5\left[Fe_{Fe}^{\bullet}\right]\right)\left(0.7 - \left[Fe_{Fe}^{\bullet}\right]\right)^2 \sqrt{pO_2}}{\left(2.9 - 0.5\left[Fe_{Fe}^{\bullet}\right]\right)\left(\left[Fe_{Fe}^{\bullet}\right]\right)^2} \tag{17}$$

Combining equation (16) and (17), $\left[Fe_{Fe}^{\bullet}\right]$ is replaced by chemical expansion:

$$K_{ox} = \frac{\left(0.1 - 0.5\frac{\varepsilon_c}{C} - 0.5 f_0\right)\left(0.7 - \frac{\varepsilon_c}{C} - f_0\right)^2 \sqrt{pO_2}}{\left(2.9 + \frac{\varepsilon_c}{C} + 0.5 f_0\right)\left(\frac{\varepsilon_c}{C} + f_0\right)^2} \tag{18}$$

Equation (18) is cubic in ε_c and thus has analytical roots. At least one real root exists and depends on the T and pO_2 parameters in the investigated range. As it is not straightforward to express the real roots as a practical relation for chemical expansion, equation (18) is approximated assuming that the chemical expansion is small, $\varepsilon_c^{\,2} << \varepsilon_c$ and $2.9 - 0.5\left(\frac{\varepsilon_c}{C} + f_0\right) \cong 2.9$, this gives the following expression:

$$2.9K_{ox}\left(\frac{\varepsilon_c}{C} + f_0\right)^2 - \left(0.1 - 0.5\left(\frac{\varepsilon_c}{C} - f_0\right)\right)\left((0.7 - f_0)^2 - 2(0.7 - f_0)\frac{\varepsilon_c}{C}\right)\sqrt{pO_2} = 0 \qquad (19)$$

This equation is quadratic for $29\,Kox + \sqrt{P}(10\,f_0 - 7) \neq 0$ or else is linear. For convenience, let's define B:

$$B = 29\,Kox + \sqrt{P}(10\,f_0 - 7) \qquad (20)$$

The physical solution gives the following relationship for chemical expansion:

$$\varepsilon_c = -\frac{1160\,f_0 Kox + \sqrt{P}A_1 - \sqrt{Kox\sqrt{P}A_2 + PA_3}}{40B}\,\mathrm{C} \text{ for } B \neq 0 \qquad (21)$$

Where P is the oxygen activity in the solid and C is the chemical expansion coefficient. Furthermore the constants A_1, A_2 and A_3, which depend on the f_0 reference concentration, are introduced.

$$\begin{cases} A_1 = 77 - 320\,f_0 + 300\,f_0^{\,2} \\ A_2 = 22736 - 46400\,f_0^{\,2} \\ A_3 = 441 + 1680\,f_0 - 2600\,f_0^{\,2} - 8000\,f_0^{\,3} + 10000\,f_0^{\,4} \end{cases} \qquad (22)$$

This system gives $A_1 = 43.6$, $A_2 = 22098.7$ and $A_3 = 591.2$. As $A_2 << A_1$ and $A_2 << A_3$ in equation (21), the chemical expansion varies mainly as a function of $(pO_2)^{1/4}$. The particular solution, for $B = 0$, is pO2=0.48 atm at 1173 K. As this model is based on the defect equilibrium (6), its domain of validity starts above 973 K.

5.2.1. Results and discussions

The exact roots of equation (18) and the solution given by equation (21) are plotted in Fig. 15 and Fig. 16. The two solutions are in good agreement.

As shown in Fig. 15, to plot the chemical expansion versus oxygen partial pressure, both the logarithm and the linear scale are relevant. At 1173 K, the chemical expansion model matches the experimental. For pO2 > 1.10^{-5} atm, chemical expansion magnitude decreases when temperature

increases. For pO2 < 1.10^{-5} atm, the maximum of chemical expansion is reached and the temperature has no influence.

Fig. 15 about here

The chemical expansion versus the temperature is illustrated in Fig. 16 for various oxygen partial pressures. The chemical expansion occurs at high temperature under oxidizing or reducing environment when reaction (6) is possible. Furthermore, at low temperature as kinetics is slow, equilibration takes more time. ΔH_0 and ΔS_0 may impact the thermal sensitivity of the chemical expansion. In H_2/H_2O, above 1073 K the chemical expansion remains constant, while in air it still increase beyond 1400 K. The chemical expansion as a function of temperature seems to be more sensitive in reducing environment because the expansion starts at lower temperature. Indeed, the more the material is oxidized the more it can be reduced when heated.

Fig. 16 about here

The chemical expansion model is plotted in a three dimensions graph as a function of oxygen activity and temperature in Fig. 17. Such representation helps to better anticipate the expansion behaviour of the membrane when changing either the temperature or the oxygen partial pressure or both simultaneously. From an initial state equilibrated in air at 1173 K (1), let's consider a thermo-chemical loading in four steps:

- Thermal loading from 1173 K to 1373 K under air: final state (1)
- Oxygen partial pressure loading from air to nitrogen at 1373 K: final state (2)
- Thermal loading from 1373 K to 1173 K under nitrogen: final state (3)
- Oxygen partial pressure loading from nitrogen to air at 1173 K: final state (4)

Fig. 17 about here

The temperature and the oxygen partial pressure can affect chemical expansion in a similar magnitude. At high temperature (e.g. 1173 K), a variation of 200 K produces a chemical expansion ($\varepsilon_{2\text{-}1}$=0.066 under air and $\varepsilon_{4\text{-}3}$=0.013 under N_2) that can be compared to the chemical expansion due to an atmosphere variation from air to nitrogen at 1373 K ($\varepsilon_{3\text{-}2}$=0.158). Tab. 2 shows a comparison between chemical expansions obtained by the model and expansion measurements. The deviation between the model and the experimental data at 1373 from air to N_2 ($\varepsilon_{3\text{-}2}$) is 7.6 % and 4.1 % at 1173 from N_2 to air ($\varepsilon_{4\text{-}1}$).

Tab. 2 about here

The effect of temperature and oxygen partial pressure should be distinguished. Indeed,

temperature changes have a direct impact on defect reaction (6) equilibrium constant (i.e., reaction (6) is shifted to the left or to the right) whereas the diffusion modifies directly the oxygen concentration in the defect reaction (6). Consequently, as shown in Fig. 18, this two variables act on the chemical expansion behaviour.

Fig. 18 about here

According to this representation, at high temperature, two situations should be considered in a membrane under operating conditions:

- Case 1: The oxygen flux is null through the membrane (oxygen activity field is homogeneous)
- Case 2: The oxygen flux is non null (oxygen activity field is heterogeneous)

In the first case, the system is in equilibrium with the surrounding atmosphere and the defect reaction (6) is only modified by temperature. This situation is encountered during the cooling steps of the non-isothermal expansion tests. In the second case, the system is not in equilibrium with the atmosphere and the defect reaction (6) may never reach equilibrium. So, the oxygen activity can be very heterogeneous in the sample. This particular situation is probably encountered during the heating steps of the non-isothermal expansion tests.

The model developed in this work provides some understanding of the chemical expansion behaviour when complex atmosphere variations occur. As in the works of Blond *and al.* and Valentin *and al.* [30, 31], the consideration of the oxygen transport phenomena would give a correct description of the expansion tests.

6. Conclusion

This work focuses on the characterization and modelling of chemical expansion of $La_{0.8}Sr_{0.2}Fe_{0.7}Ga_{0.3}O_{3-\delta}$. The nature of chemical strain in MIECs working under oxidizing and reducing atmospheres has been studied with the help of TGA, XRD and expansion measurements in a wide range of temperatures (RT, 1473 K) and oxygen partial pressure (1 atm, 10^{-19} atm). The XRD and expansion give values of chemical expansion as a function of oxygen partial pressure. The TGA measurements give the oxygen vacancies concentration in relation to the temperature and the oxygen partial pressure. A classical defect model was used to determine the concentration of different possible defects. It is shown that the chemically-induced strain is not linearly dependent on the oxygen non-stoechiometry but depends on $\left[Fe_{Fe}^{4+}\right]$ concentration. A model of chemical expansion as a function of T and pO_2 is proposed by solving the equation of the defect reaction Fe^{3+}/Fe^{4+}. The approached solution shows an excellent agreement with the analytical solution and the chemical

expansion measurements at high temperature. The definition domain of the model is limited to high temperatures without diffusion process. Its relative complexity could condemn it as an engineering tool for large-scale membrane reactor. However, this kind of model provides a better understanding of the chemical expansion behaviour when complex variations of the operating parameters occur.

Acknowledgements

The authors acknowledge Air Liquide and ADEME for supporting this research.

References

[1] U. Balachandran, J. T. Dusek, R. L. Mieville, R. B. Poeppel, M. S. Kleefisch, S. Pei, T. P. Kobylinski, C. A. Udovich, and A. C. Bose. Applied Catalysis A: General, 133 (1995) 19

[2] H. J. M. Bouwmeester, Catalysis Today, 82 (2003) 141

[3] S.J. Feng, S. Ran, D.C. Zhu, W. Liu, and C.S. Chen. Energy Fuels, 18 (2004) 389

[4] G. Etchegoyen, T. Chartier, and P. Del-Gallo. Journal of Solid State Electrochemistry, 10 (2006) 597

[5] E. Juste. PhD thesis (in French), Université de Limoges, 2008.

[6] A. Julian, E. Juste, P.M. Geffroy, N. Tessier-Doyen, P. Del Gallo, N. Richet, and T. Chartier. Journal of the European Ceramic Society, 29 (2009) 2603

[7] T. R. Armstrong, J.W. Stevenson, L.R. Pederson, and E.R Paige. Journal of The Electrochemical Society, 143 (1996) 2919

[8] V. V. Kharton, A. A. Yaremenchecko, M. V. Patrakeev, E. N. Naumovich, and F. M. B. Marques. Journal of the European Ceramic Society, 23 (2003) 1417

[9] S. Pei, M. S. Kleefisch, T. P. Kobylinski, J. Faber, C. A. Udovich, V. Zhang-Mccoy, B. Dabrowski, U. Balachandran, R. L. Mieville, and R. B. Poeppel. Catalysis Letters, 30 (1995) 201

[10] K. E. Colombo, V. V. Kharton, and O. Bolland. Energy & Fuels, 24 (2010) 590

[11] P. H. Larsen, P. V. Hendriksen, and M. Mogensen. Journal of Thermal Analysis and Calorimetry, 49 (1997) 1263

[12] M. V. Patrakeev, E. B. Mitberg, A. A. Lakhtin, I. A. Leonidov, V. L. Kozhevnikov, V. V. Kharton, M. Avdeev, and F. M. B. Marques. Journal of Solid State Chemistry, 167 (2002) 203

[13] F. Boroomand, E. Wessel, and H. Bausinger. Solid State Ionics, 129 (2000) 251

[14] A. Atkinson and T. M. G. M. Ramos. Solid State Ionics, 129 (2000) 259

[15] K. Garikipati, L. Bassman, and M. Deal. Journal of the Mechanics and Physics of Solids, 49 (2001) 1209

[16] X. Chen, J. Yu, and S. B. Adler. Chemistry of Materials, 17 (2005) 4537

[17] N. Swaminathan and J. Qu. Fuel Cells, 7 (2007) 453

[18] X. Dong, Z. Xu, X. Chang, C. Zhang, and W. JIN. Journal of the American Ceramic Society, 90 (2007) 3923

[19] R. Krishnamurthy and B. W. Sheldon. *Acta Mater.*, 52 (2004) 1807

[20] S. B. Adler. Journal of the American Ceramic Society, 84 (2001) 2117

[21] A. Le Bail, H. Duroy, and J.L. Fourquet. Materials Research Bulletin, 23 (1988) 447

[22] A. Julian, E. Juste, P.M. Geffroy, V. Coudert, S. Degot, P. Del Gallo, N. Richet, and T. Chartier. Journal of Membrane Science, 333 (2009) 132

[23] M. Sogaard, P. V. Hendriksen, and M. Mogensen. Journal of Solid State Chemistry, 180 (2007) 1489

[24] P. V. Hendriksen, P. H. Larsen, M. Mogensen, F. W. Poulsen, and K. Wiik. Catalysis Today, 56 (2000) 283

[25] J.W. Stevenson, T.R. Armstrong, L.R. Pederson, W.J. Weber, H.U. Anderson, A.C. Khandkar, and M. Liu. Proceedings of the First International Symposium on Ceramic Membranes, The Electrochemical Society, Proc. ,95-24 (1995) 94

[26] J. Mizusaki, N. Mori, H. Takai, Y. Yonemura, H. Minamiue, H. Tagawa, M. Dokiya, H. Inaba, K. Naraya, T. Sasamoto, and T. Hashimoto. Solid State Ionics, 129 (2000) 163

[27] A. Fossdal, M. Menon, I. Woernhus, K. Wiik, M.-A. Einarsrud, and T. Grande. Journal of the American Ceramic Society, 87 (2004) 1952

[28] J. Mizusaki, M. Yoshihiro, S. Yamauchi, and K. Fueki. Journal of Solid State Chemistry, 58 (1985) 257

[29] A. Zuev, L. Singheiser, and K. Hilpert. Solid State Ionics, 147 (2002) 1

[30] E. Blond and N. Richet. Journal of the European Ceramic Society, 28 (2008) 793

[31] O. Valentin, E. Blond, A. Julian, and N. Richet. Computational Materials Science, 46 (2009) 912

Figure Caption list and Table Caption list.

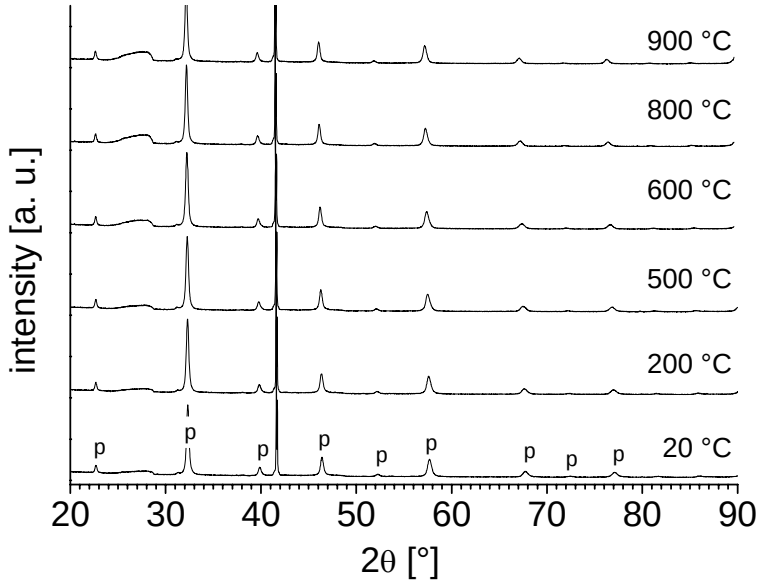

Fig. 1. XRD patterns for $La_{0.8}Sr_{0.2}Fe_{0.7}Ga_{0.3}O_{3-\delta}$ under air from 293 to 1173 K, letter p stands for the perovskite phase

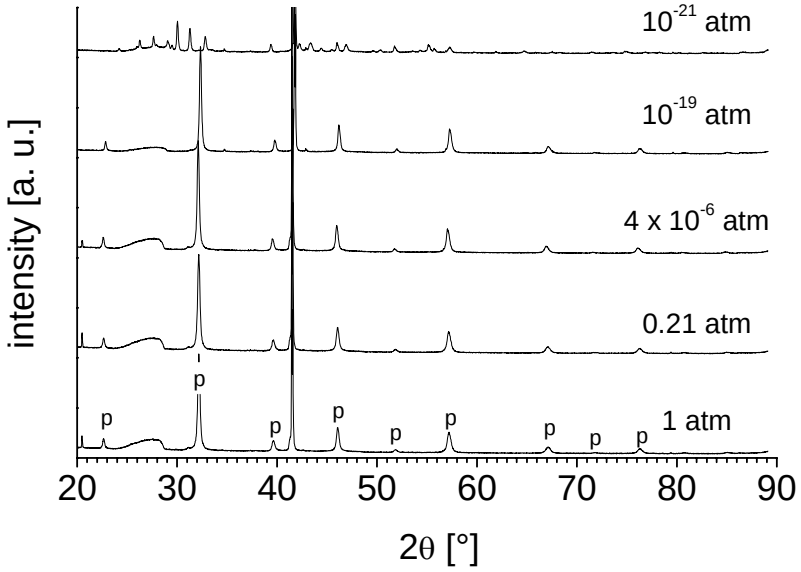

Fig. 2. Example of XRD patterns for $La_{0.8}Sr_{0.2}Fe_{0.7}Ga_{0.3}O_{3-\delta}$ at 1173 K under various oxygen atmospheres, letter p stands for the perovskite phase

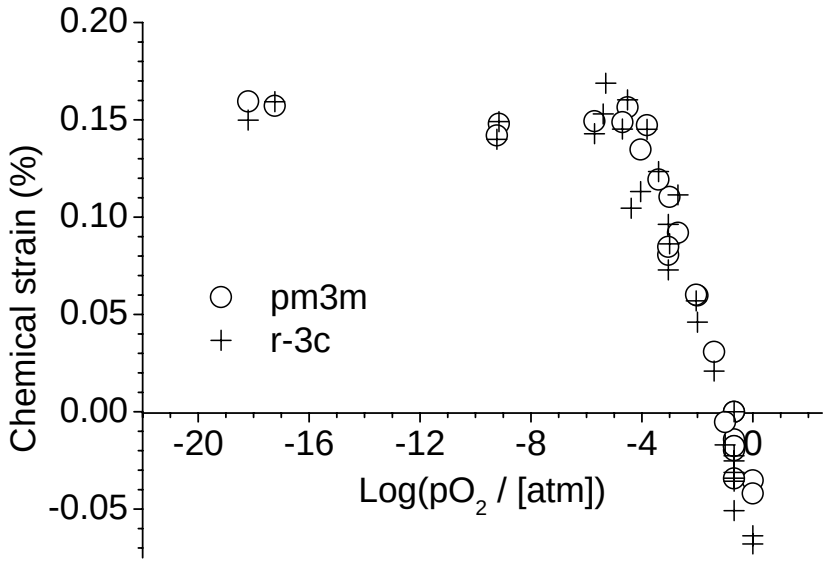

Fig. 3. Chemical expansion by XRD obtained from the two space group

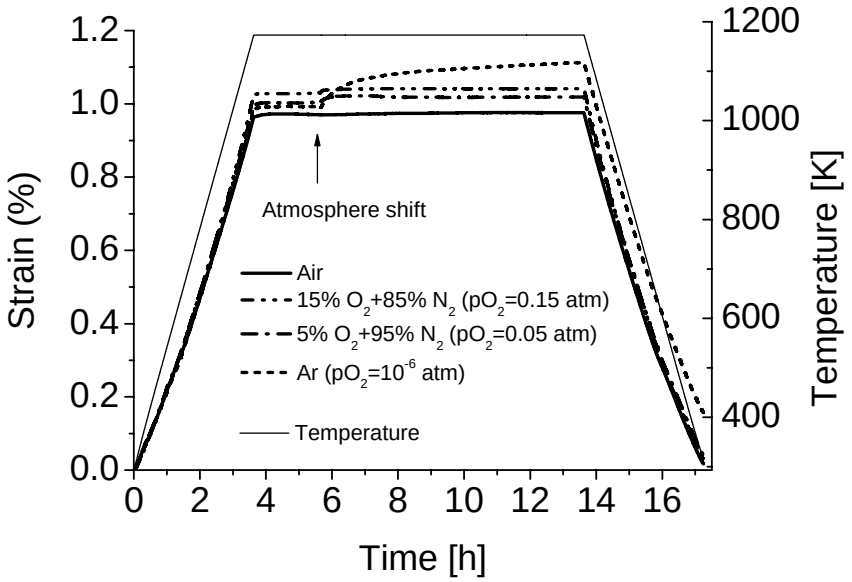

Fig. 4. Isothermal dilatometry at 1173 K for LSFG

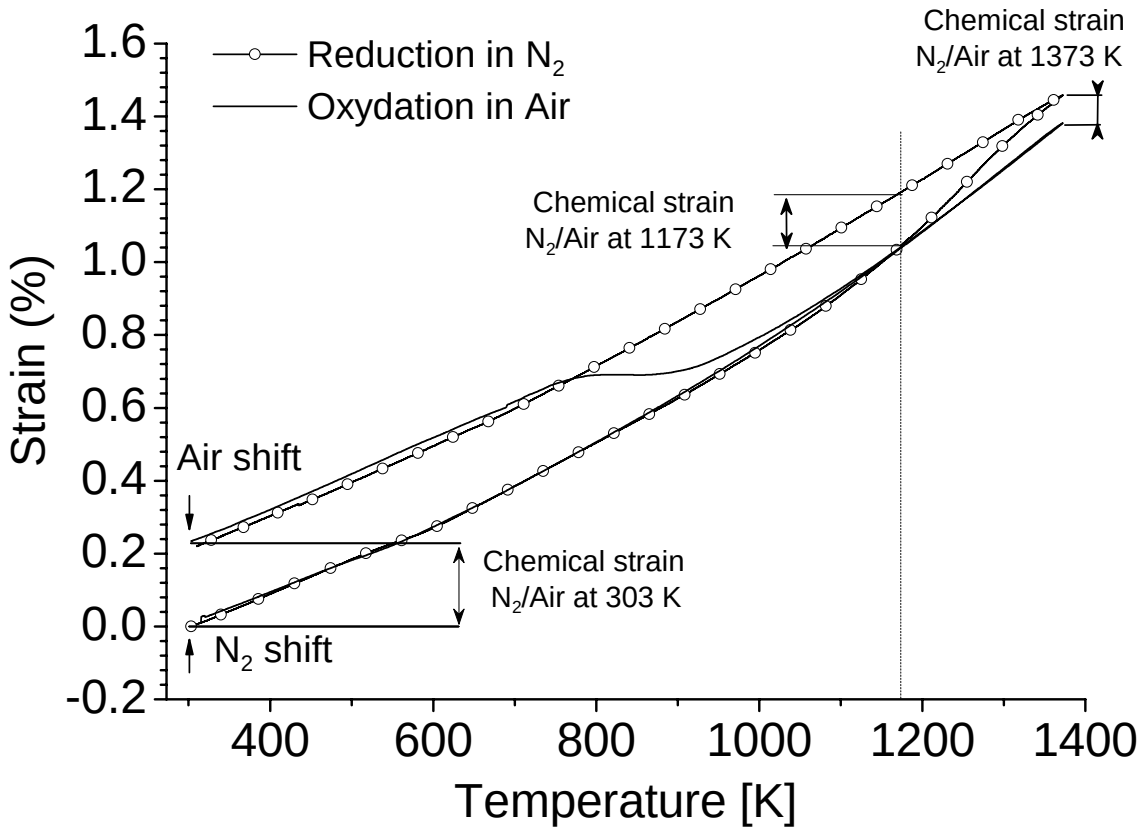

Fig. 5. Thermo-chemo dilatometry for LSFG under N_2 then Air

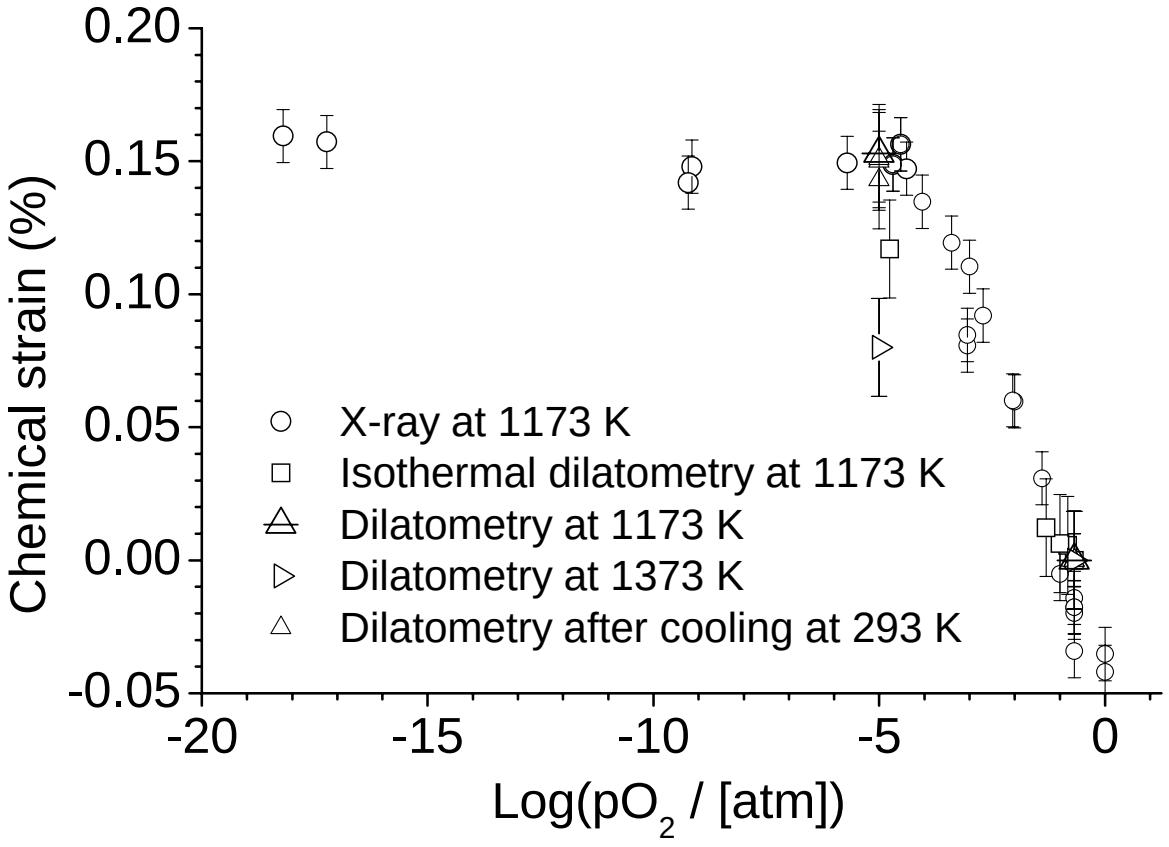

Fig. 6. Chemical expansion by X-ray and dilatometry measurements as a function of log pO_2

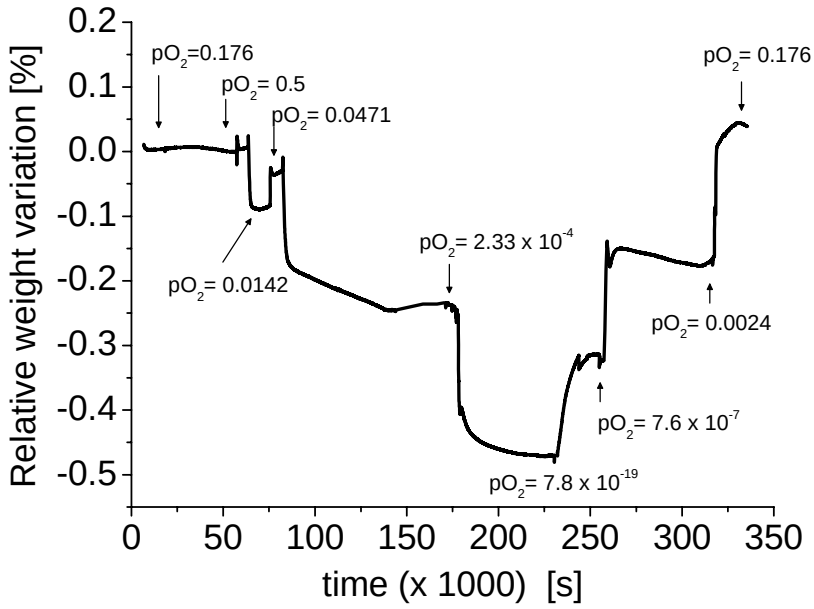

Fig. 7. Relative weight variation in relation to various oxygen partial pressures by thermogravimetry at 1173 K

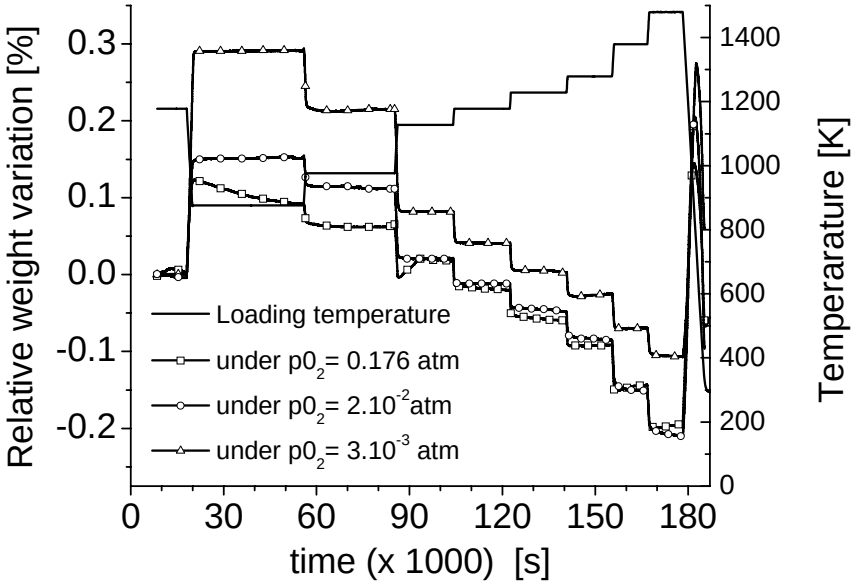

Fig. 8. Relative weight variation in relation to temperature under 0.176, 2 x 10^{-2} and 3 x 10^{-3} atm

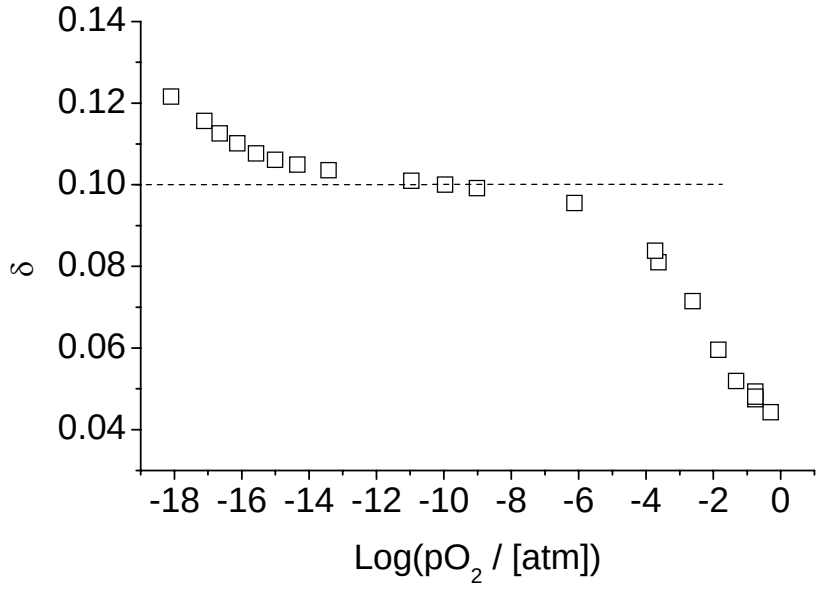

Fig. 9. Oxygen non-stoichiometry as a function of log pO_2 for $La_{0.8}Sr_{0.2}Fe_{0.7}Ga_{0.3}O_{3-\delta}$ at 1173 K

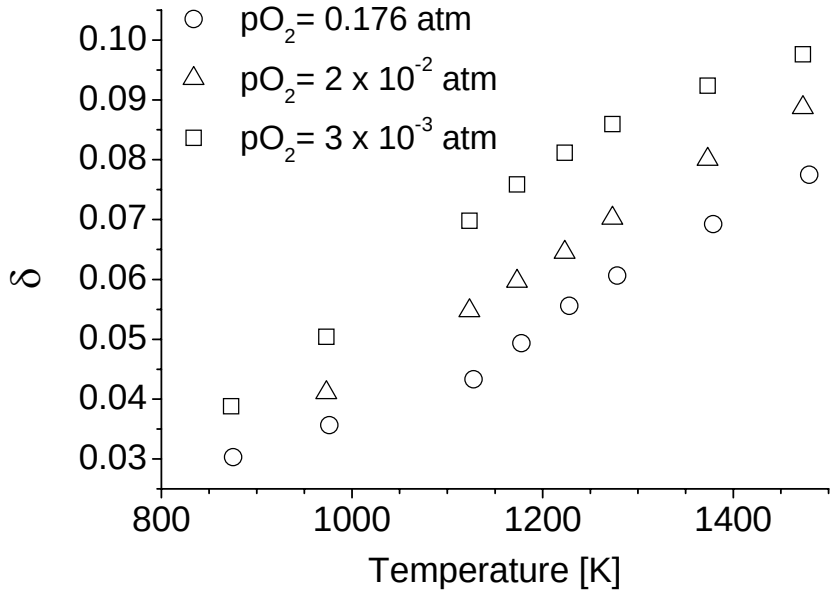

Fig. 10. Oxygen non-stoichiometry in relation to temperature under 0.176, 2 x 10^{-2} and 3 x 10^{-3} atm

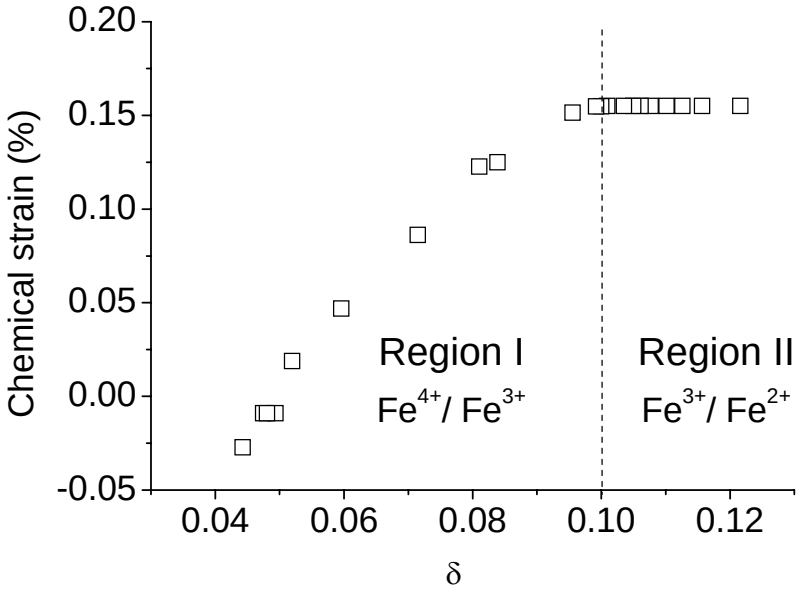

Fig. 11. Chemical expansion as a function of oxygen vacancy concentration δ for LSFG8237 at 1173 K

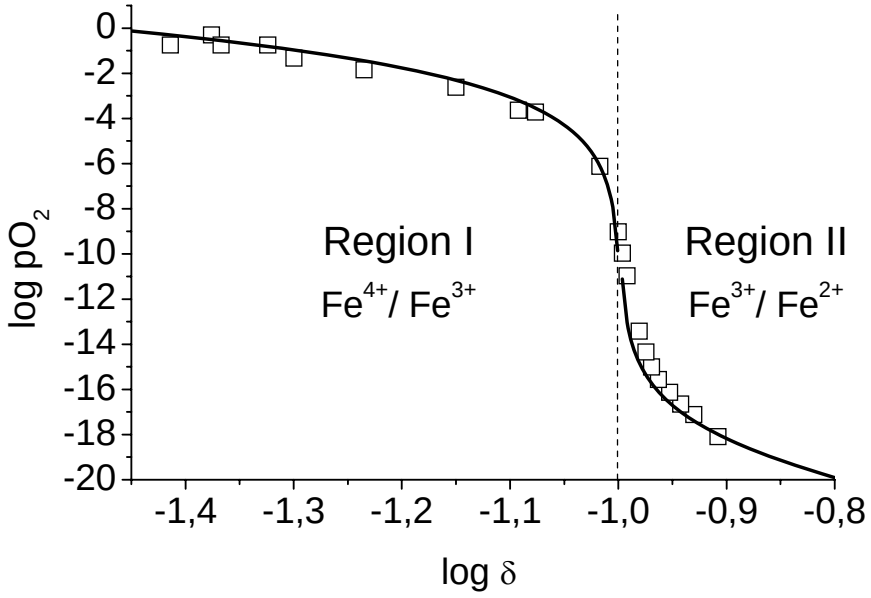

Fig. 12. log pO_2 vs. log δ diagram and fitting curves with K_{ox} and K_{red} at 1173 K

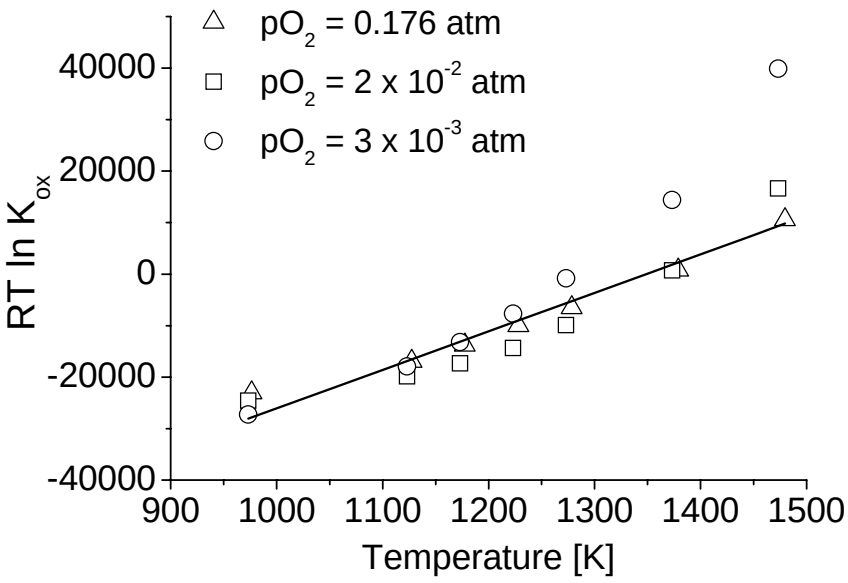

Fig. 13. Standard Gibbs free energy change as function of temperature for three different oxygen partial pressures 0.176, 2 x 10^{-2} and 3 x 10^{-3} atm

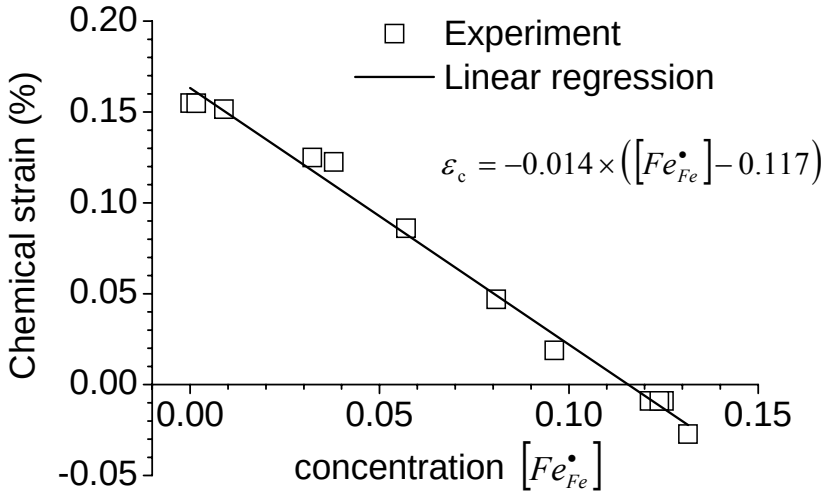

Fig. 14. Chemical expansions *vs.* $\left[Fe'_{Fe} \right]$ concentration at 1173 K

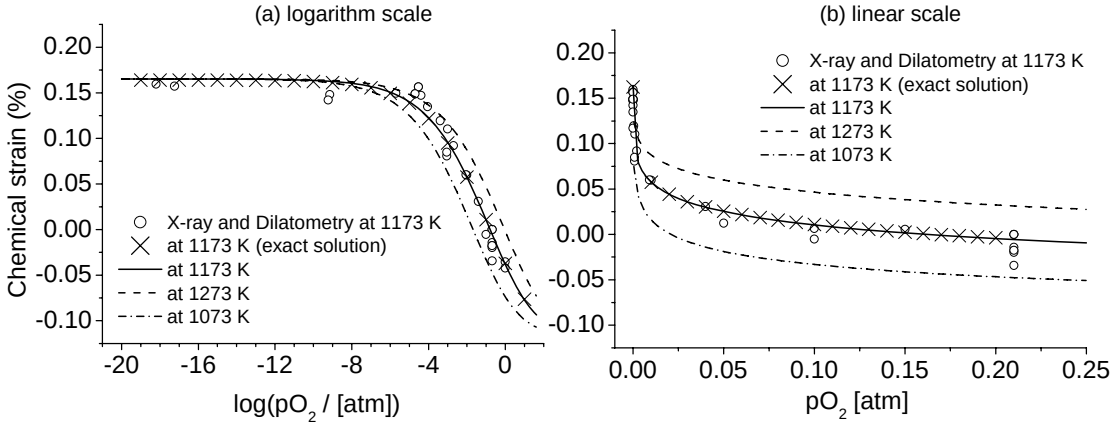

Fig. 15. Chemical expansion vs. oxygen partial pressure at 1273, 1173 and 1073 K, (a) logarithm scale, (b) linear scale

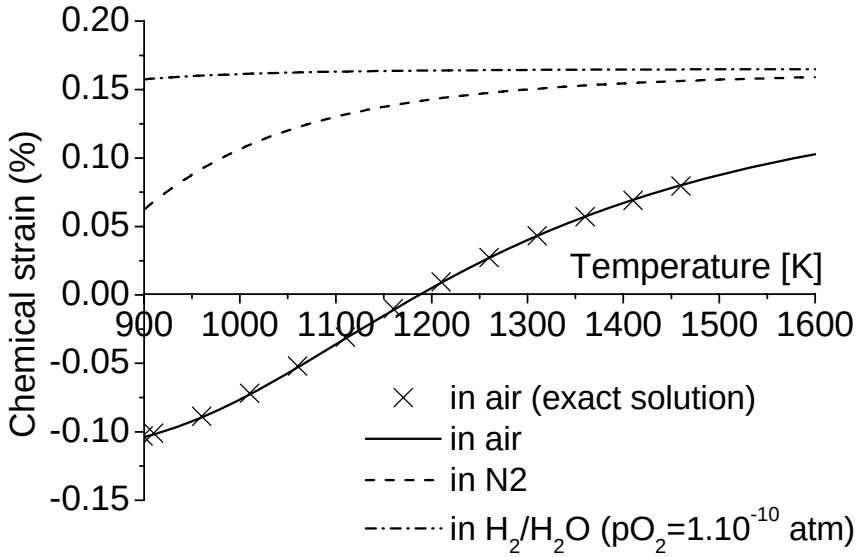

Fig. 16. Chemical expansion model *vs.* temperature under Air, Nitrogen and H_2/H_2O

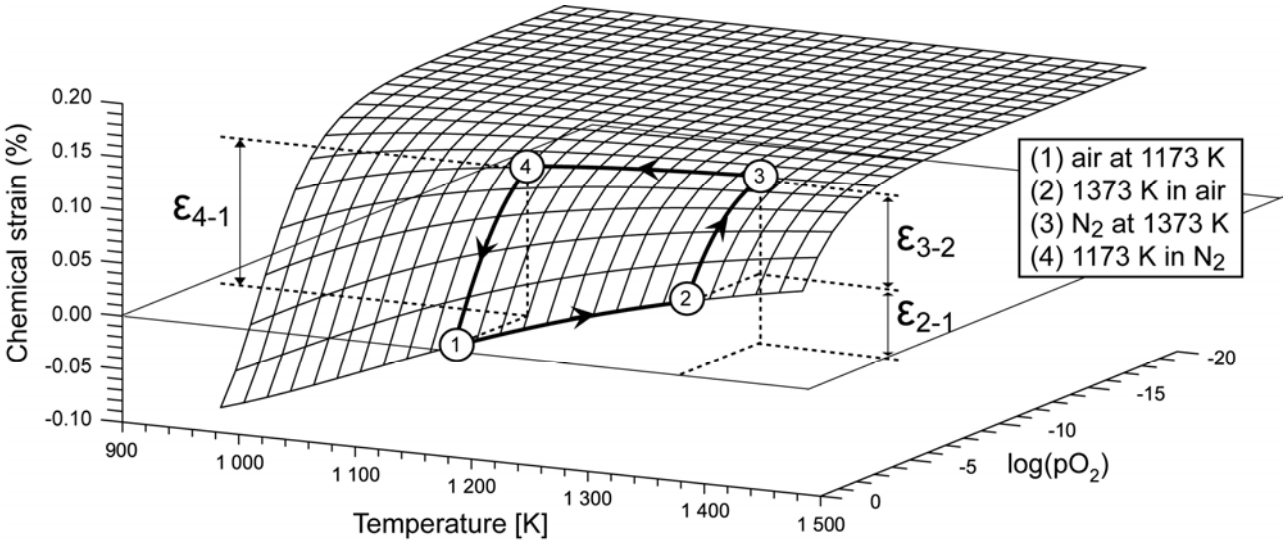

Fig. 17. Chemical expansion as function of oxygen partial pressure and temperature

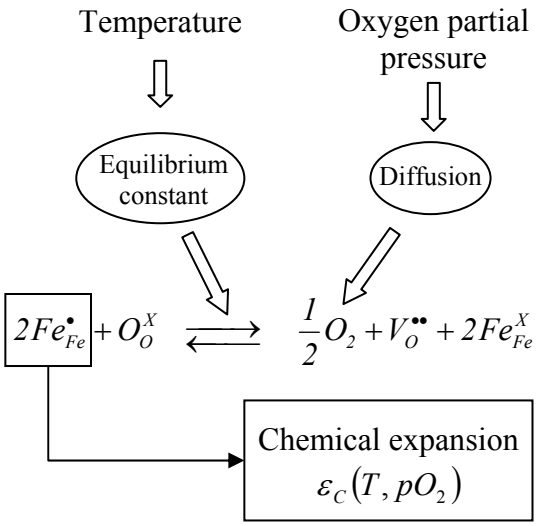

Fig. 18. Schematic representation of the origin of influence of the oxygen partial pressure and temperature on the chemical expansion

ΔH_0 [kJ.mol^{-1}]	ΔS_0 [J.mol^{-1}.K]	Material and Author
107 ±10	75 ±5	$La_{0.8}Sr_{0.2}Fe_{0.7}Ga_{0.3}O_{3-\delta}$ [This study]
97.5	67.7	$La_{0.6}Sr_{0.4}Fe0_{3-\delta}$, [28]

Tab. 1 Average standard enthalpy and entropy changes of the reaction (6) in [1100; 1300] K under oxygen partial pressures 0.176, 2 x 10^{-2} and 3 x 10^{-3} atm

Expansion	Conditions		Chemical expansion ε_C [%]		Deviation
	Temperature	pO_2	Model	Experiment (dilatometry from Fig. 5)	
ε_{3-2}	1373	Air→N_2	0.092	0.085	7.6 %
ε_{4-1}	1173	N_2→Air	0.145	0.151	4.1 %

Tab. 2 Chemical expansion obtained by the model and the dilatometries